

# Photonic crystal optics in cold atomic gases

Marina Litinskaya, Evgeny A. Shapiro

*Department of Chemistry, University of British Columbia, Vancouver, V6T 1Z1, Canada*

We describe propagation of light in a gas with periodic density modulation, demonstrating photonic-crystal-like refraction with negative refraction angles. We address the role of poorly defined boundaries and damping, and derive an optical analog of the quantum adiabatic theorem. For Cs atoms in an optical lattice, we show that relying on semi-adiabatic propagation one can excite and spatially split positively and negatively refracting modes at experimentally available gas densities.

PACS numbers: 78.20.Ci, 37.10.Jk, 42.70.Qs

**Introduction.** A wave is negatively refracted at an interface of two media if its group velocity component along the interface changes its sign [1], see Fig. 1(a). Fascinating optical effects based on negative refraction (NR) include invisibility [2], near-field focusing with planar devices [3], seeing around a corner [4], and superprism [5]. This work is aimed at achieving similar effects in a gas. Using laser fields instead of nanofabrication for preparing the sample will enable dynamical real-time control at a distance in the optical frequency domain [6, 7]. New applications such as nonlinear spectroscopy with backward propagating signal [8] may become available.

Photonic-crystal (PC) metamaterials offer a route to NR [9]. Both negatively and positively refracted modes appear due to periodic modulation of the dielectric constant, see Fig.1(b). We shall call them “N-” and “P-” modes, respectively, implying both the negative-like refraction in 1D PCs and true NR in 2D, where Snell’s law with a negative refractive index is in effect [10]. Below we theoretically demonstrate the possibility of negative-like refraction in a cold gas trapped in an optical lattice. Photonic band gap is routinely observed in such systems [11]. We study NR in the proof of principle case of 1D periodicity; implementation in 2D and 3D is straightforward. The scheme offers relatively low gas densities, simple design, and a large frequency window of negative refraction.

Implementation in a gas brings two challenges absent in solid materials. First, due to low densities, a significant modulation of the dielectric constant is only possible in a narrow vicinity of a resonance, where absorption is high. This resonant absorption can be overcome using schemes based on Electromagnetically Induced Transparency (EIT) [12]. Here we study another route: For a thermal gas trapped in a 1D optical lattice, we consider relatively large detuning from the resonance so that both absorption and modulation of the refractive index are moderate. The negative-like refraction emerges due to periodicity of the lattice potential. In this arrangement, the required gas density turns out to be experimentally achievable  $10^{13} \text{ cm}^{-3}$  [13], three to five orders of magnitude lower than in the earlier proposals [6, 7]. As discussed below, the advantage comes both from not relying on the weak magnetic response of the gas, and from the N-mode being immune to resonant absorption.

The second challenge, common for all gaseous samples and never treated before, is due to poorly defined boundaries in a gas cloud. If light penetrates the cloud adiabatically, then only P-mode is excited and negative refraction is never achieved. Below we derive an analog of the quantum adiabatic theorem for coupled propagation of N- and P-modes, and study the dynamics of energy transfer between them. We show that with experimentally achievable conditions one can realize propagation possessing both adiabatic and non-adiabatic features, thus providing transfer into the N-mode, and simultaneously avoiding unwanted reflection at boundaries.

**Waves in resonant periodic arrays.** A 1D PC with a period  $a$  comparable with a half of the light wavelength  $\lambda$  (Fig. 1(b)) acts as a volume diffraction grating and supports P- and N-diffracted modes [10, 14]. We model an infinite (so that the boundary is irrelevant) grating as a periodic set of delta-like perturbations in the dielectric constant:

$$\varepsilon(z; \omega) = 1 + \varepsilon_c d \sum_n \delta(z - na) = 1 + \frac{d}{a} \varepsilon_c \sum_n e^{inzG}. \quad (1)$$

Here  $G = 2\pi/a$ , and  $\varepsilon_c$  is the dielectric contrast between the layers of the grating and vacuum. Applying modal approach [15], we find an analytical solution for the Maxwell equations for TE-polarized waves,  $\mathbf{E} = (0, E, 0)$ ,  $\mathbf{H} = (H_x, 0, H_z)$ , as follows. Due to periodicity along  $z$ , the eigenstates are Floquet-Bloch (FB) modes [14] consisting of partial waves (marked by index  $m$ ) of the form

$$E(z; t) = \sum_m C_m \exp \left[ i(k_x x + (k_z + mG)z - \omega t) \right], \quad (2)$$

with the amplitudes  $C_m$  obtained by substituting (1) and (2) into the Maxwell wave equation:

$$C_m = \frac{\varepsilon_c \omega^2 (\sum_l C_l)}{c^2 [k_x^2 + (k_z + mG)^2] - \omega^2}. \quad (3)$$

The values  $\omega$ ,  $k_x$  and  $k_z$  satisfy the dispersion equation, obtained by summing (3) over  $m$  and cancelling  $\sum_m C_m$  and  $\sum_l C_l$ . The remaining sum over  $m$  can be calculated analytically. We write the result as:

$$\cos ak_z = \cos ak_z^{(vac)} - \frac{d}{a} \frac{\varepsilon_c}{2} \left( \frac{\omega a}{c} \right)^2 \frac{\sin ak_z^{(vac)}}{ak_z^{(vac)}}, \quad (4)$$

where  $k_z^{(vac)} = \sqrt{\frac{\omega^2}{c^2} - k_x^2}$ . FB modes of the form (2-3) are sketched in Fig. 1(b). The arrows show phase velocity directions. The group velocity is the same for all partial waves in a mode. Amplitude of  $m$ -th partial wave is determined by the corresponding denominator in RHS of Eq.(3), i.e. by how close to  $\omega^2/c^2$  each  $k_x^2 + (k_z + mG)^2$  is, and is shown schematically by the arrow thickness.

The number of different FB modes with the same value of  $k_z$  and their propagation directions can be deduced from the equi-frequency surface (EFS) for Eq.(4) in the  $k_x, k_z$  plane [10, 14, 15]. Fig. 1(c) shows an example EFS for the frequency  $\omega = 1.25\pi c/a$  and strong modulation of  $\varepsilon$ . The periodicity results in the EFS diagram with the property  $\omega(k_x, k_z) = \omega(k_x, k_z + mG)$  for all  $m$ : instead of a single circle  $k_x^2 + k_z^2 = \omega^2/c^2$  (green dashed circle in the figure), EFS consists of a series of circles corresponding to different partial waves. In addition, the modulation opens Bragg gaps at  $k_z = G/2 + mG$ , which change the topology of the EFS: Instead of intersecting circles corresponding to the bare photon dispersion repeated along  $k_z$ , there is a series of smaller inner ellipses embraced by merging outer parts of the circles. Each FB mode of the PC is characterized by a specific value of  $k_x$ , and a set of  $k_z = k_{z0} + mG$ ,  $m = 0, \pm 1, \pm 2, \dots$ . In Fig. 1(c) they are represented by points on the EFS. Points C and C' belong to the same mode: C marks its partial wave with  $m = 0$ , C' marks  $m = -1$ .

Consider a light beam incident from  $x = -\infty$  at an angle  $\phi$  as shown in Fig.1(b). This beam is represented by point A on the green dashed circle  $\sqrt{k_{x0}^2 + k_{z0}^2} = \omega/c$  in Fig.1(c). At the boundary, it can couple to all the FB modes with the same value of  $k_{z0} = (\omega/c) \sin \phi$ . Intersections of the line  $k_z = k_{z0}$  (dotted blue line) with the EFS determine the  $k_x$  values of the eigenmodes coupled to the probe. Normals to the EFS (depicted by arrows in Fig. 1(c)) determine the group velocity directions of these modes [10, 14, 15]. Figure shows that for  $k_{z0}$  close to  $\pi/a$  there are two normal modes with positive  $x$ -component of the group velocity: an N-mode (with  $k_x \equiv k_N$ , point C) and a P-mode (with  $k_x \equiv k_P$ , point B). Note that the N-mode exhibits negative-like refraction. Points D and E with the same  $k_{z0}$  and  $k_x = -k_{N,P}$  correspond to two reflected waves, marked as  $N_{ref}$  and  $P_{ref}$ .

The size of the gap at  $k_z = \pi/a$  is determined by the value of  $\varepsilon_c$  in Eq.(1). In conventional PCs, the contrast  $\varepsilon_c$  comes from remote resonances (background dielectric constant). In a gas with the mean density  $\rho$ , substantial contrast appears only near an atomic resonance,  $\omega_T$  [16]:

$$\frac{d}{a}\varepsilon_c \rightarrow \varepsilon_{res}(\omega) = \frac{8\pi\omega_T\mu^2\rho}{\omega_T^2 - \omega^2 - 2i\omega_T\gamma}, \quad (5)$$

where  $\mu$  is the dipole transition matrix element, and  $\gamma$  accounts for losses. Below we imply that the periodic structure shown on Fig. 1(b) depicts atoms in a 1D optical lattice. The calculations are done for the D2 line of Cs ( $\mu = 4.48$  a.u.,  $\omega_T = 11732$  cm $^{-1}$ ) with  $\rho = 10^{13}$  cm $^{-3}$  [13] in a lattice with  $a = 532$  nm. Both the Doppler and

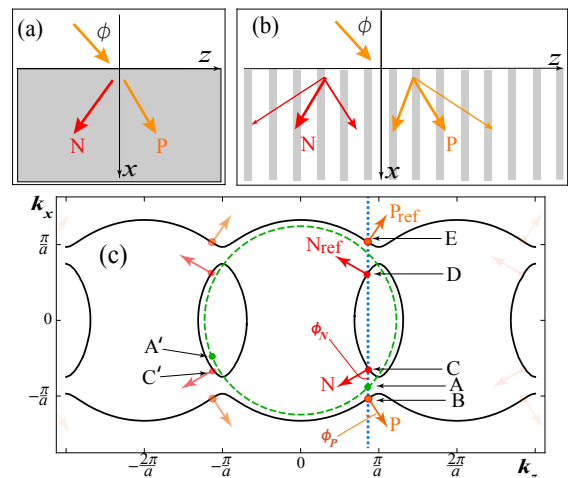


FIG. 1: (Color online) (a) Negative (red) and positive (gold) refraction at an interface. (b) Negative and positive Floquet-Bloch modes in a 1D photonic crystal. (c) Solid black line: EFS in a 1D PC. Green dashed circle: EFS for light in vacuum. Red and gold arrows show the propagation directions of the N- and P-modes. Points A, A' mark the incident and outgoing light beams in free space, as discussed in the text. Points B, C, D, E mark the P-, N-,  $N_{ref}$ - and  $P_{ref}$ -modes.

collisional widths at  $T < 1$  K are negligible compared to the radiative broadening  $\gamma \simeq 33$  MHz [17].

**Dynamics of coupled modes at the boundary.** Inside the gas cloud, the dielectric contrast is a function of the penetration depth:  $\varepsilon_{res}(x, \omega) = \alpha(x)\varepsilon_{res}(\omega)$ . Here  $\alpha(x)$  is the density profile characterized by two scales: the total length of the cloud  $L$ , and the length of the entrance and exit zones,  $L_*$ . In these zones  $\alpha(x)$  varies between 0 (vacuum) and 1 (saturated density). Each value of  $x$  can be assigned its own EFS diagram. As  $x$  grows, EFS gradually transforms from a single circle  $\sqrt{k_x^2 + k_z^2} = \omega/c$  to a periodic structure similar to that shown in Fig. 1(c) by the thick black line. The free-space mode shown by point A adiabatically connects upon such gradual transformation with the P-mode characterized by the same value of  $k_z$  (point B). If the gas density at the boundary changes slowly, then transfer of energy from the P-mode both to the (wanted) N-mode (point C), and (unwanted) reflected modes (points D and E) is suppressed.

We look for the field  $E(x, z)$  inside the cloud in the form of a superposition of the N- and P-modes. Coupling to the reflected modes is neglected on the basis of higher adiabaticity, as explained below. Thus

$$E = \sum_{Y=N,P} c_Y(x) |Y(x)\rangle e^{i \int_0^x \Re k_Y(x_1) dx_1}, \quad (6)$$

where  $\Re k_Y = \text{Re}[k_Y]$  for  $Y = N, P$  is the real part of  $k_x = k_{N,P}$  found from Eq.(4).  $|Y(x)\rangle$  stands for the N- and P-eigenmodes of the type (2) calculated in the local basis: At each  $x$ , the amplitudes  $C_m(x)$  of the partial waves are related to the wave vector components

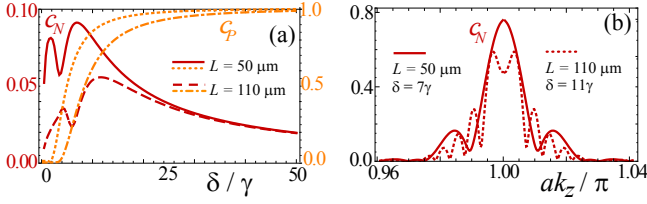


FIG. 2: (Color online) (a) Amplitudes  $|c_P(L)|$  (gold, right scale) and  $|c_N(L)|$  (red, left scale) in dependence on  $L$  and  $\delta$  with  $L_* = 20 \mu\text{m}$ . (b)  $|c_N(L)|$  at  $x = L$  as a function  $k_z = \omega/c \sin \phi$  for two sets of parameters.

$k_z, k_Y(x)$  as in Eq.(3) with  $\varepsilon_c$  replaced by  $\alpha(x)\varepsilon_{\text{res}}(\omega)$ . For the  $|N(x)\rangle$  mode we further denote  $C_m \rightarrow N_m(x)$ , and for the  $|P(x)\rangle$  mode  $C_m \rightarrow P_m(x)$ . The damping enters through  $\text{Im}[k_{N,P}(x)]$ , and leads to decline of the amplitudes  $c_N$  and  $c_P$  as  $x$  grows. Each eigenmode is normalized as  $\langle Y|Y \rangle \equiv \sum_m |Y_m|^2 = 4\pi\omega/c^2 \mathfrak{K}_Y$  [18]. This normalization corresponds to a unit energy flow across the plane  $x = \text{const}$  for zero damping.

To find the amplitudes  $c_N(x)$  and  $c_P(x)$  across the sample, we substitute Eq.(6) into the wave equation with  $\varepsilon(x, z, \omega) = \alpha(x)\varepsilon(z, \omega)$ , and apply the slow envelope approximation [16], assuming that the  $x$ -derivatives of  $c_N(x)$ ,  $c_P(x)$ ,  $N_m(x)$ ,  $P_m(x)$  are all small compared to  $\mathfrak{K}_N, \mathfrak{K}_P$ . Using the fact that the vectors  $|N\rangle, |P\rangle$  are the solutions of the wave equation at a fixed  $x$ , we obtain:

$$\begin{aligned} & \left[ 2\mathfrak{K}_N c'_N |N\rangle + 2\mathfrak{K}_N c_N |N'\rangle + (\mathfrak{K}'_N + i(\mathfrak{K}_N^2 - k_N^2)) c_N |N\rangle \right] \\ & \times e^{i \int_0^x dx_1 \mathfrak{K}_N(x_1)} + \left[ 2\mathfrak{K}_P c'_P |P\rangle + 2\mathfrak{K}_P c_P |P'\rangle \right. \\ & \left. + (\mathfrak{K}'_P + i(\mathfrak{K}_P^2 - k_P^2)) c_P |P\rangle \right] e^{i \int_0^x dx_1 \mathfrak{K}_P(x_1)} = 0 \end{aligned} \quad (7)$$

where “ $'$ ” stands for  $x$ -derivative. Multiplying (7) consecutively by  $\langle N|$  and  $\langle P|$  we find [21]:

$$\begin{aligned} c'_N &= \xi^* \mathfrak{K}_P c_P \exp \left[ i \int_0^x (\mathfrak{K}_P - \mathfrak{K}_N) dx_1 \right] - i\eta_N \mathfrak{K}_N c_N \quad (8) \\ c'_P &= -\xi \mathfrak{K}_N c_N \exp \left[ -i \int_0^x (\mathfrak{K}_P - \mathfrak{K}_N) dx_1 \right] - i\eta_P \mathfrak{K}_P c_P, \end{aligned}$$

where (note that  $\text{Im}[\eta_Y \mathfrak{K}_Y] = -\text{Im}[k_Y]$ )

$$\xi = \frac{c^2}{4\pi\omega} \langle P|N'\rangle, \quad \eta_Y = \frac{c^2}{4\pi\omega} \text{Im}[\langle Y|Y'\rangle] + \frac{1}{2} \left( 1 - \frac{k_Y^2}{\mathfrak{K}_Y^2} \right). \quad (9)$$

Eqs.(8) resemble the equations describing two-state quantum dynamics with the time derivative replaced by  $x$ -derivative. We draw an analogy with the quantum adiabatic theorem [22] by noticing that coupling between the modes averages out if  $|\xi \mathfrak{K}_{P,N}| \ll |\mathfrak{K}_P - \mathfrak{K}_N|$  at all  $x$ . When damping is negligible,  $\eta_N \approx \eta_P \approx 0$ , the analogy can be further developed by noticing that  $\langle P|N'\rangle$  is estimated as  $\pi\varepsilon_{\text{res}}\omega/(2vL_*(k_P^2 - k_N^2))$  with

$v = 1/|\sum_{mn} P_m^* N_n|$  [23]. Using this estimate, we obtain the adiabaticity condition as

$$\Omega_A \equiv L_*(k_P - k_N)^2 \frac{16v}{\omega\varepsilon_{\text{res}}} \gg 1, \quad (10)$$

$\Omega_A$  is the adiabaticity parameter. The transfer between the modes only takes place if their wave vectors are sufficiently close. The latter observation allowed us to neglect the reflected modes in Eq.(6): At the values of  $L_*$  such that the evolution of coupled P- and N-modes corresponding to points B, C in Fig. 1(c) is barely non-adiabatic, coupling to the reflected modes corresponding to the points D, E can be neglected due to larger  $|k_P - k_{P_{\text{ref}}, N_{\text{ref}}}|$ . This is different from conventional PCs, where reflection at the boundary is always present.

**Numerical results and discussion.** For light entering the sample, equations (8) are solved numerically with the boundary conditions  $c_N(0) = 0$ ,  $c_P(0) = 1$ . The amplitude  $c_N(L)$  at the exit depends on four key parameters. On one hand,  $L_*$ ,  $k_z = (\omega/c) \sin \phi$  and the detuning  $\delta = \omega - \omega_T$  determine the adiabaticity parameter  $\Omega_A$ . On the other hand,  $\delta$  and  $L$  determine losses due to absorption. The smaller is  $\delta$ , the larger is the (wanted) dielectric contrast and (unwanted) absorption. In Fig.2(a) we plot the amplitudes at the exit,  $|c_N(L)|$ ,  $|c_P(L)|$ , as functions of  $\delta$  for  $L = 50$  and  $110 \mu\text{m}$ , with  $L_* = 20 \mu\text{m}$ ,  $\rho = 10^{13} \text{cm}^{-3}$ ,  $k_z = 0.98\pi/a$ , and  $\alpha(x) = 1$  inside the cloud and changing according to  $\sin^2(\pi x/2L_*)$  law at the boundaries. The amplitude  $c_N(L)$  reaches values  $0.05 \div 0.1$  in the frequency window as large as  $20\gamma$ , i.e. over 2.5 GHz, slowly declining at larger detunings. For strong absorption ( $\delta < 2\gamma$  for our geometry), coupling between the modes is only effective at the entrance: The P-mode is completely absorbed at  $x \lesssim L_*$ , see the dynamics of  $c_{P,N}(x)$  in Fig.3(c). The N-mode survives, experiencing much lower absorption, due to reasons discussed below. In the regime of small absorption ( $\delta > 20\gamma$ )  $c_P(L) \simeq 1$ , and  $c_{P,N}(L)$  do not depend on  $L$ . We observed that at higher densities the energy transfer dynamics strongly resembles that in a Landau-Zener transition [24]. At intermediate absorption, the values  $c_P(L)$  and  $c_N(L)$  are comparable. Fig.2(b) shows the angular dependence of  $|c_N(L)|$  and  $|c_P(L)|$  calculated for the same density profiles as in Fig.2(a). The value  $k_z = 0.98\pi/a$ , used in the rest of our calculations for illustrative purposes, is at the edge of the window of allowable angles. Closer to the Bragg angle,  $|c_N(L)|$  can be as high as 0.8.

Figure 3 illustrates propagation of a Gaussian beam with the central wave vector  $k_z = 0.98\pi/a$ ,  $\delta = 2\gamma$ , through a cloud with  $L_* = 20 \mu\text{m}$ ,  $L = 50 \mu\text{m}$ . The intensities of the two modes in Panel (d) are calculated by expanding the initial Gaussian beam into plain waves, each with its own  $k_x, k_z$ . For each of them we write the field as in Eqs.(3,6), and propagate it according to Eqs.(8). Then we combine the waves to retrieve the overall field. The resulting angles of propagation of the P- and N-beams,  $\phi_N$  and  $\phi_P$ , correspond to the curvature

of the EFS at points B,C in Fig. 1(c).

According to Panels (a) and (c), transfer between the modes is only efficient for  $x \leq 10 \mu\text{m}$ , where the distance between  $\mathfrak{K}_N$  and  $\mathfrak{K}_P$  is minimal and dynamics have non-adiabatic features, cf. Eq.(10). The P-mode is completely absorbed inside the cloud, and only the N-mode is present at the exit. As the gas density at the exit of the cloud decreases, all the amplitudes  $N_m$  except  $N_{-1}$ , depicted by point C' in Fig. 1(c), vanish. Due to partial adiabaticity of the exit dynamics, C' connects with A' on the green circle, and the N-mode leaves the cloud in such a way that its NR-like propagation is preserved.

Panel (b) of Fig.3 illustrates a key ingredient of our scheme. As the gas density increases,  $\text{Im}[k_P]$  increases as well, but  $\text{Im}[k_N]$  quickly reaches maximum and stabilizes. The closer  $k_z$  to  $\pi/a$  or the higher gas density, the smaller  $\text{Im}[k_N]$ . From Eq.(3), near  $k_z \simeq \pi/a$  the partial wave amplitudes  $P_m, N_m$  with  $m = 0, -1$  are large, and all others are small. For the N-mode  $N_0 \simeq -N_{-1}$ , whereas  $P_0 \simeq P_{-1}$  [25]. Stabilization of the asymmetric N-mode can be attributed to destructive interference: the field maxima are at the  $z$  values with no lattice atoms. For the symmetric P-mode, the field maxima coincide with the lattice density maxima, and absorption is high. This phenomenon can be described [26] in the language similar to that of many interference phenomena in quantum mechanics [27]. The absence of absorption in the N-mode allows choosing small detunings from the resonance, thus weakening the requirement for the gas density.

Fig.4 shows propagation of the same Gaussian beam as in Fig.3 for intermediate absorption,  $\delta = 3\gamma$  and  $7\gamma$ . By varying the detuning, one can control the P-mode exit intensity while keeping the N-mode intact. For a large detuning and low absorption (Panels (c), (d)), non-adiabaticity of the exit with  $L_* = 20 \mu\text{m}$  begins to play a role: The amplitude  $c_N$  grows both at the entrance and at the exit from the cloud. Counterintuitively, the N-mode is generated in the regions of low, rather than high, gas density – i.e. where adiabaticity is low.

**In conclusion**, our scheme realizes NR-like light

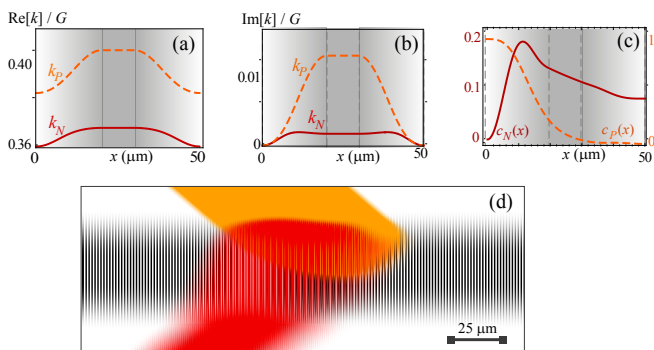


FIG. 3: (Color online) Strong absorption ( $\delta = 2\gamma$ ). Spatial dependence of the real (a) and imaginary (b) parts of  $k_N$  and  $k_P$ , and of  $c_N$  and  $c_P$  (c). Dashed vertical lines mark the entrance and exit zones. (d) Beam propagation through the cloud. Gold shows P-beam, red – N-beam.

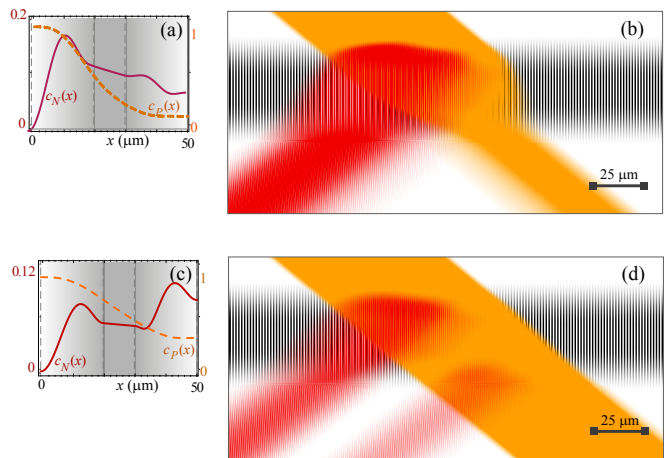


FIG. 4: (Color online) Same as in Fig.3 (c,d), but for intermediate and weak absorption:  $\delta = 3\gamma$  (a,b), and  $\delta = 7\gamma$  (c,d).

propagation in a cold gas at the experimentally achieved density of  $10^{13} \text{ cm}^{-3}$ . This density estimate is three orders of magnitude lower than in the chirality-based proposals [7], and five orders of magnitude lower than in magnetic resonance-based proposals [6]. The advantage is due to the PC-like structure being induced via strong electric-dipole couplings in atoms, as compared to weak magnetic-dipole couplings required in previous schemes. Stabilization of the N-mode against absorption further weakens the density requirements. Finally, due to the effect of the grating, a very weak contrast of  $\varepsilon$  (in our calculations,  $\varepsilon_c \sim 10^{-2}$ ) is sufficient for strong modification of light propagation. At the same time, bandwidth of the NR window is  $\sim 20$  times higher than the frequency window in EIT-based bandgap structures [12].

Implementation of our scheme in higher-dimensional lattices with true negative refraction is straightforward. In conventional PCs, high dielectric contrast is required to avoid the unwanted positively refracted wave [10]. The present scheme can be employed even with small  $\varepsilon_c$ , since the birefringence is suppressed via absorption of the P-mode. Vaguely defined boundaries make the dynamics of light conceptually different from that at a conventional interface. However, with reasonable length parameters one can transfer noticeable fraction of light into the N-mode while fully controlling intensity of the P-mode at the exit. Intensity of the negatively refracted light will be higher for higher gas densities, smaller absorption, and angles closer to the Bragg angle.

**Acknowledgements.** The authors dedicate this work to the memory of Moshe Shapiro. His insight stimulated our work on negative refraction in gases.

We are pleased to thank M. Sukharev and K. Madison for consultations.

- [1] “Physics of negative refraction and negative index materials”, C. M. Krowne and Y. Zhang (eds.), Springer, 2007.
- [2] J. Pendry, *Physics*, **2**, 95 (2009); Y. Lai et al, *Phys. Rev. Lett.*, **102**, 253902 (2009).
- [3] V. G. Veselago, *Sov. Phys. Uspekhi*, **10**, 509 (1968); J. B. Pendry, *Phys. Rev. Lett.*, **85**, 3966 (2000); P. V. Parimi, W. T. Lu, P. Vodo, S. Sridhar, *Nature* **426** 404 (2003).
- [4] See <http://skullsinthestars.com/2009/05/19/what-does-negative-refraction-look-like/> and references therein.
- [5] H. Kosaka et al., *Phys. Rev. B* **58**, R10096 (1998).
- [6] M. Ö. Oktel, Ö. E. Müstecaplıoğlu, *Phys. Rev. A*, **70**, 053806 (2004).
- [7] J. Kästel, M. Fleischhauer, S. F. Yelin, R. L. Walsworth, *Phys. Rev. Lett.*, **99**, 073602 (2007); D. E. Sikes, D. D. Yavuz, *Phys. Rev. A* **82**, 011806(R) (2010).
- [8] V. E. Kravtsov, V. M. Agranovich, K. I. Grigorishin, *Phys. Rev. B*, **44**, 4931 (1991).
- [9] E. Cubukcu, K. Aydin, E. Ozbay, S. Foteinopoulou, C.M. Soukoulis, *Nature* **423**, 604 (2003). For a review, see S. Foteinopoulou, *Physica B* **407**, 4056 (2012) and references therein.
- [10] M. Notomi, *Phys. Rev. B* **62**, 10696 (2000); S. Foteinopoulou, C. M. Soukoulis, *Phys. Rev. B* **72**, 165112 (2005).
- [11] G. Birkl, M. Gatzke, I. H. Deutsch, S. L. Rolston, W. D. Phillips, *Phys. Rev. Lett.* **75**, 2823 (1995); I. H. Deutsch, R. J. C. Spreeuw, S. L. Rolston, W. D. Phillips, *Phys. Rev. A* **52**, 1394 (1995); A. Schilke, C. Zimmermann, P. W. Courteille, W. Guerin *Phys. Rev. Lett.* **106**, 223903 (2011).
- [12] A. Andre and M. D. Lukin, *Phys. Rev. Lett.* **89**, 143602 (2002); D. Petrosyan, *Phys. Rev. A* **76**, 053823 (2007); M. Artoni and G.C. La Rocca, *Phys. Rev. Lett.* **96**, 073905 (2006); Y. Zhang *et. al*, *Op. Ex.* **21**, 29338 (2013).
- [13] C. Chin, A. J. Kerman, V. Vuletić, S. Chu, *Phys. Rev. Lett.*, **90**, 033201 (2003).
- [14] P. St. J. Russel, *Appl. Phys. B*, **39**, 231 (1986).
- [15] R. S. Chu and T. Tamir, *Proc. IEEE*, **119**, 197 (1972); R. S. Chu, J. A. Kong, *IEEE Trans. of Microwave Theory and Techniques*, **MTT-25**, 18 (1977).
- [16] L. Allen, J. H. Eberly, “Optical resonance and two-level atoms” (Wiley-Interscience, New York, 1975).
- [17] Daniel A. Steck, Cesium D Line Data, available online at <http://steck.us/alkalidata> (revision 2.0.1, 2 May 2008).
- [18] We adopt “bra” and “ket” notations of conventional quantum mechanics. Alternatively, one can use the formalism of biorthogonal states, see e.g. N. Moiseyev, “Non-Hermitian quantum mechanics”, (Cambridge University Press, Cambridge, 2011) and Refs.[19, 20].
- [19] M. V. Fedorov, M. A. Efremov, V. P. Yakovlev, W. P. Schleich, *JETP* **97**, 522 (2003).
- [20] O. Atabek and R. Lefebvre, *J. Phys. Chem. A* **114**, 3031 (2010).
- [21] We used the relations  $\text{Re}[\langle Y|Y'\rangle] = -2\pi\omega\Re_Y'/c^2\Re_Y^2$  and  $\langle N|P'\rangle = \langle P'|N\rangle^* = -\langle P|N'\rangle^*$ , obtained by differentiating  $\langle Y|Y\rangle = 4\pi\omega/c^2\Re_Y$  and  $\langle P|N\rangle = 0$  over  $x$ .
- [22] M. S. Sarandy and D. A. Lidar, *Phys. Rev. A* **71**, 012331 (2005); A. Fleischer and N. Moiseyev, *Phys. Rev. A* **72**, 032103 (2005); M. H. S. Amin, *Phys. Rev. Lett.* **102**, 220401 (2009).
- [23] We introduce a local-basis wave operator  $\hat{L}(x) = \partial^2/\partial z^2 + \varepsilon(z, \omega)\omega^2/c^2$ . At a given  $x$ ,  $\hat{L}(x)|N(x)\rangle = k_N^2(x)|N(x)\rangle$ ; similar for  $|P\rangle$  and  $k_P$ . We differentiate the last equation over  $x$ , multiply the result by  $\langle P|$  and use the wave equation for the P-mode  $\langle P|\hat{L} = k_P^2\langle P|$ . We then replace  $\langle P|\hat{L}'|N\rangle$  by  $\alpha'\langle P|\varepsilon(\omega, z)|N\rangle = \alpha'\varepsilon_c \sum_{nm} P_m^* N_n$ . For the density profile used in the calculations, we replace  $\alpha'$  by  $\pi/2L_*$ , and notice that in the regions of low adiabaticity  $k_P \simeq k_N$ , and  $|k_{P,N}/(k_P + k_N)| \simeq 1/2$ .
- [24] Q. Niu and M. G. Raizen, *Phys. Rev. Lett.* **80**, 3491 (1998).
- [25] The sign of the amplitude  $C_m$  depends on that of the denominator in Eq.(3). The latter can be visualized using Fig. 1(c), and depends on whether the point on EFS, which corresponds to the  $m$ -th partial wave, is inside or outside the green dashed circle with the radius  $\omega/c$ . For the N-mode, point C representing the  $0^{th}$  partial wave is inside the circle, and point C' representing the  $-1^{st}$  wave is outside. Thus the signs of  $N_0$  and  $N_{-1}$  are different. For the P-mode, both  $0^{th}$  and  $-1^{st}$  partial waves are represented by points outside the green circle, and the signs of  $P_0$  and  $P_{-1}$  coincide.
- [26] See M. V. Berry, D. H. J. O'Dell, *J. Phys. A: Math. Gen.*, **31**, 2093 (1998). To compare with our case, one must assume complex  $\sigma$  in Eq.(8), and replace in Eq.(12)  $\sigma/2$  by  $\sigma$  to account for  $\delta(x)$ -like instead of cos-like perturbation.
- [27] The stabilization phenomenon is described in Ref.[26] in terms of the amplitudes of  $0^{th}$  and  $-1^{st}$  partial waves coupled via the lattice. Compare, e.g., with strong-field interference stabilization in M. V. Fedorov, N. P. Poluektov, A. M. Popov, *et. al.*, *IEEE J. Sel. Papers on Quantum Electronics* **18**, 42 (2002); formation of dark states via interference and EIT in M. Shapiro and P. Brumer, “Quantum Control of Molecular Processes” (Wiley-VCH, Weinheim, 2012) and M. Fleischhauer, A. Imamoglu, J. P. Marangos, *Rev. Mod. Phys.* **77**, 633 (2005), as well as stabilization of atoms passing through an optical lattice in [19] and resonances of dissociating molecules in [20].